Dynamics of the Proton Transfer Reaction on the Cytoplasmic Surface of Bacteriorhodopsin†

Sharon Checover, Yael Marantz, Esther Nachliel, and Menachem Gutman*

Laser Laboratory for Fast Reactions in Biology, Department of Biochemistry, Tel Aviv University, Tel Aviv 69978, Israel

Matthias Pfeiffer, Joerg Tittor, and Dieter Oesterhelt

Max-Planck-Institut für Bochemie, Martinsried D-82152, Germany

Norbert A. Dencher

Technische Universitat Darmstadt, Institut fur Biochemie, Darmstadt D-64287, Germany

Received November 7, 2000; Revised Manuscript Received February 9, 2001

ABSTRACT: The cytoplasmic surface of bacteriorhodopsin is characterized by a group of carboxylates that function as a proton attractive domain [Checover, S., Nachliel, E., Dencher, N. A., and Gutman, M. (1997) *Biochemistry 36*, 13919−13928]. To identify these carboxylates, we selectively mutated them into cysteine residues and monitored the effects of the dynamics of proton transfer between the bulk and the surface of the protein. The measurements were carried out without attachment of a pH-sensor to the cysteine residue, thus avoiding any structural perturbation and change in the surface charge caused by the attachment of a reporter group, and the protein was in its BR state. The purple membranes were suspended in an unbuffered solution of pyranine (8-hydroxypyrene-1,3,6-trisulfonate) and exposed to a train of 1000 laser pulses (2.1 mJ/pulse, $\lambda = 355$ nm, at 10 Hz). The excitation of the dye ejected the hydroxyl's proton, and a few nanoseconds later, a pair of free protons and ground-state pyranine anion was formed. The experimental observation was the dynamics of the relaxation of the system to the prepulse state. The observed signals were reconstructed by a numeric method that replicates the chemical reactions proceeding in the perturbed space. The detailed reconstruction of the measured signal assigned the various proton-binding sites with rate constants for proton binding and proton exchange and the p*K* values. Comparison of the results obtained by the various mutants indicates that the dominant proton-binding cluster of the wild-type protein consists of D104, E161, and E234. The replacement of D104 or E161 with cysteine lowered the proton binding capacity of the cluster to ∼60% of that of the native protein. The replacement of E234 with cysteine disrupted the structure of the cluster, causing the two remaining carboxylates to function as isolated residues that do not interact with each other. The possibility of proton transfer between monomers is discussed.

Membrane proteins are made of tight structures of α-helices or *β*-sheets that are interconnected by loops more exposed to the bulk. The membrane-crossing sections of proteins are enriched by nonpolar residues, while the charged residues are concentrated on the interconnecting loops. These residues on the loops serve both as electrically interacting elements that stabilize the structure and for short- and long-range interactions with the substrate. In the study presented here, we monitored the reaction of the exposed residues with free diffusing proton, using the velocity to the reaction to gauge its accessibility of the surface groups, and the inter-relation between them.

The protein selected for study was bacteriorhodopsin, a light-driven, vectorial proton pumping protein with a well-studied structure and an established mechanism of reaction. In recent years, there has been much progress in the elucidation of its three-dimensional structure, and a few structural models were resolved, derived either by electron and X-ray diffraction of two-dimensional crystals in membranes (*2*−*5*) and three-dimensional crystals (*6*−*12*) or by atomic force microscopy (*13*, *14*). The derived structures are in good agreement with respect to their cross-membranal sections. Yet, the interconnecting loops are not well resolved (*15*). In some models, sections of the loops could not be observed or were defined with a large temperature factor. As for the C-terminal section, the last 10−15 residues are missing from all present structures. Accordingly, it appears that in solution, regions on the surface loops are in a very dynamic state and should better be described in terms of a population of states rather than as a single conformation.

The inability to resolve the dynamic structure of a protein, by averaging observations such as diffraction techniques, can be partially overcome by the application of time-resolved observations that gauge the relative orientation of the surface groups by measuring the rate of a defined chemical reaction.

† This research is supported by the German-Israeli Foundation for Scientific Research and Development (GIF) (Grant I-140-207.98) and the United States-Israel Binational Science Foundation (BSF) (Grant 97-130).

* To whom correspondence should be addressed. E-mail: me@hemi.tau.ac.il.

10.1021/bi002574m CCC: $20.00
Published on Web 03/15/2001

In previous studies (*1*, *16*, *17*), we had measured the protonation dynamics of the surface of bacteriorhodopsin preparations, labeled by a fluorescein molecule on either the extracellular or the cytoplasmic side of the purple membrane (PM).[1] The dynamics were monitored at two wavelengths that recorded the state of protonation of two pH indicators, pyranine in the aqueous bulk phase and a surface-bound fluorescein. The observation was initiated by a short laser pulse that temporarily offset the acid−base equilibrium, and the response of the system to the perturbation was monitored over time. The observed signals were subjected to a kinetic analysis that quantitated the rate constants of all proton transfer reactions between the bulk and surface, as well as the rates of proton exchange reactions between sites on the protein. According to this analysis, only six of the many surface carboxylates interacted with protons on the microsecond time scale, the range in which proton binding and release are operative. The other surface carboxylates are probably located close to positive charges, which lower their p*K* values. These acidic carboxylates do bind the free proton, but keep them for such a short time that the microsecond dynamic is unaffected. Five of these carboxylates are located on the cytoplasmic face of the membrane and one on its extracellular side. Two of the fast-reacting carboxylates on the cytoplasmic side were identified as D36 and D38 (*1*, *18*), and the rate of proton exchange between them was found to be extremely fast, with a virtual rate constant (*19*) of $\sim 10^{12}$. The other three carboxylates of the cytoplasmic surface appeared to form a cluster of closely arranged residues that merged their coulomb cages into a common proton attractive site. The cluster was characterized by a p*K* of 5.5 and an exceptionally fast rate of reaction with free protons ($k = 4 \times 10^{10}$ M^{-1} s^{-1}) (*1*, *16*, *17*). This rate is comparable to the rate of protonation of the highly charged ($Z = -4$), free diffusing pyranine anion. In the study presented here, the identity of the cluster is investigated.

The experimental algorithm we employed was a systematic replacement of each surface carboxylate with cysteine and measurements of the effects of the replacement on the transient proton binding capacity of the protein in the microsecond time range. The photocycle of these mutants was studied by Riesle et al. (*18*) and Brown et al. (*20*), an observation which is a much more complex system than the present one. Under physiological conditions, the bacteriorhodopsin functions at a high salt concentration and against a heavy $\Delta\mu H^+$ backpressure. The understanding of the mechanism under these conditions calls for a preliminary studies of the proton transfer reactions under simpler conditions. For these reasons, our study was carried out at a low salt concentration, in the absence of electrochemical gradients, while the protein is in its most prevalent conformation, the BR state. To avoid further complexities, we decided to sacrifice the experimental convenience of attaching a fluorescein to the cysteine residue (*1*, *17*), thus avoiding the possible deformation of the structure by the extra charges of the indicator. Therefore, the only stress imposed on the mutated protein was caused by the substitution of the residues under study with an uncharged residue.

[1] Abbreviations: pyranine or ϕOH, 8-hydroxypyrene-1,3,6-trisulfonate; BR, light-adapted state of bacteriorhodopsin; PM, purple membrane.

The kinetic features of the various mutated surfaces were studied by the laser-induced proton pulse (*1*, *17*, *19*, *21*, *22*). The protein was suspended in a dilute solution of pyranine and excited by a short laser pulse. Following excitation, the dye dissociated to ϕO^- and H^+, where the incremental concentration of the former was directly monitored at 458 nm. By following the dynamics of the dye's reprotonation, we could differentiate between the various proton-binding sites on the protein's surface, assigning specific kinetic and thermodynamic parameters to each. In the first part of the investigation, we demonstrated how the various proton-binding sites of the wild-type protein can be identified and characterized by reconstructing the observed signals. Thereafter, the same algorithm was used for the study of the mutated proteins, and the carboxylates that form the highly reactive cluster were identified as D104, E161, and E234.

MATERIALS AND METHODS

Proton Pulse Technique. The experimental observation consists of a δ-function perturbation of the acid−base equilibrium in the solution, attained by a UV laser pulse (355 nm, 3 ns fwhm, 1.4−2.1 mJ/pulse operating at 10 Hz) that excites the pyranine to its first electronic singlet state. In its excited state, the p*K* falls to a p*K** of 1.4 and the hydroxyl's proton dissociates with a time constant of ~120 ps. Following the relaxation of the dye to the ground state ($\tau \sim 5$ ns), the system is poised in a temporary state of disequilibrium, where both free proton and ϕO^- concentrations are above the equilibrium level, while the ϕOH population is transiently depleted. This initial perturbation propagates to all other proton-binding sites present in the pulsed solution through a diffusion-controlled reaction with the photodissociation products (H^+ and ϕO^-). The response of the system to the perturbation proceeds through many parallel pathways, where the velocity of each reaction is determined by the concentrations of the reactants and the respective rate constants. The kinetic and stoichiometric coupling between all reactants implies that a followup of one reactant would yield information concerning the state of protonation of all others.

Proteins, as polyelectrolytes, are thermodynamically coupled, and the protonation of any site can affect the p*K* of other sites (*23*). Thus, when a protein is challenged by a large proton pulse, its thermodynamic and kinetic characteristics may vary during the reaction time. To avoid these complications, the experiments were carried out under the limitation that the incremental proton concentration was lower than the total protein concentration, ensuring that each protein molecule reacts with no more than a single proton.

Instrumental Setup. The optical geometry and electronic setup were as previously described (*17*). Pyranine (8-hydroxypyrene-1,3,6-trisulfonate, laser grade) was purchased from Eastman Kodak (Rochester, NY).

Mutagenesis and Expression. Site-specific mutants of bacteriorhodopsin were prepared according to the method of Ferrando (*24*). Mutagenesis was followed by transformation and homologous expression in *Halobacterium salinarum* strains HN5 and L33, with the help of the shuttle plasmid pEF 191. Mutated proteins were isolated as purple membrane sheets according to the method of Oesterhelt and Stoeckenius (*25*).

Preparation of the Sample. Purple membranes were extensively washed with pure water by three repeated

Table 1: Rate Constants[a] of Protonation of Bicarbonate and Its Collisional Proton Transfer Reaction with the Pyranine Anion

pK	$HCO_3^- + H^+$	$HCO_3^- + \phi O^-$
6.3	$(2.8 \pm 0.2) \times 10^{10}$	$(3.0 \pm 1) \times 10^8$

[a] All rate constants are given in the units of M^{-1} s^{-1}.

centrifugations to remove buffers, and the mercaptoethanol that was added to prevent the oxidation of the SH residues introduced by mutagenesis. The PMs were suspended to a final concentration of 3−20 μM in an unbuffered pyranine solution (20−30 μM). The dynamics were measured within the pH range of 6−8 and at varying protein/pyranine ratios. The measured signals are an average of 1024 traces.

The carboxyl groups of Glu74, Glu234, and Asp38 in bacteriorhodopsin were modified by 1-ethyl-3-[3-(dimethylamino)propyl]carbodiimide (EDC) according to the method of Renthal et al. (*26*).

At low protein concentrations, it is necessary to account for the presence of bicarbonate generated by equilibration with the atmospheric CO_2. A complete elimination of CO_2 from the system was very laborious, and in most cases, there was some re-accumulation during the observation. For this reason, we preferred to pre-equilibrate the system with air and to determine the bicarbonate concentration in the reaction mixture by measuring the dynamics of pyranine in the absence of protein at fixed time intervals during the experimental session. Thus, the concentration was determined by the same method used for the analysis of the results. We noticed that the bicarbonate content was constant during the full duration of the experiment. The contribution of bicarbonate, determined for each experimental session, was incorporated in the kinetic analysis of the data. The kinetic and thermodynamic parameters characterizing the bicarbonate reaction with free protons, pyranine anion, and the carboxylates on the BR are listed in Table 1. In all figures, the mathematically reconstructed dynamics were calculated with the bicarbonate content pertinent to the experimental session.

Kinetic Analysis of the Absorbance Signals. The experimental curves were analyzed by a detailed reconstruction of the dynamics response of all chemical reactions to the acid−base perturbation, the reprotonation of the pyranine anion, and the reversible protonation of the surface groups of the membrane (*27*). The proton-binding sites at the membrane were treated separately, as were those located on the extracellular face of the membrane (COO^-_{EC}) and sites on the cytoplasmic face of the membrane (COO^-_{CP}) (*1*, *17*). Each of the surface reactants can exchange a proton with the free-diffusing pyranine anion and among each other. To convert the multiequilibrium system into a kinetic model, all the reactions were combined into a set of coupled, nonlinear, parametric differential rate equations, which complied with the detailed balance principle. The integration over time of these equations reproduced the relaxation dynamics of all components in the system.

The integration over time of the differential rate equations by a numeric procedure reconstructed the chemical events associated with the perturbation relaxation of the system. Thus, by providing the program with the specific concentrations of the reactants and a set of rate constants, we can mathematically reconstruct the observed dynamics. For each protein preparation, we analyzed a large number of independently measured signals, in a search for a set of parameters that would reconstruct them all.

The differential rate equations and the integration program are available upon request.

RESULTS

Effect of the Laser Flash on the Bacteriorhodopsin. An experimental system in which two photoreactive compounds are present is inherently complex. Both the pyranine and the bacteriorhodopsin can enter their respective photocycles. For this reason, it was imperative to determine which fraction of the BR is activated during the proton pulse experiment. The probing of a photoreactive protein, such as BR, by another photochemical reaction (photodissociation of pyranine) can be carried out only when the cross correlation between them is well established. In this case, it is not only the UV flash (355 nm) that might activate the retinal but also the intensive emission from the excited pyranine at a λ_{max} of 515 nm, a wavelength at which the cross section of the retinal is much higher, that may drive the protein into its photocycle. To quantitate this fraction, we carried out a measurement (in the presence of BR and pyranine) while monitoring the solution at 528 nm. At this wavelength, the dissociation of the pyranine has a negligible absorption change, but the BR photocycle is well resolved. These measurements revealed that less than 1% of the BR was driven into its photocycle. Thus, we are confident that the reactions described below characterize the proton transfer reactions on the surface of the protein in its BR state.

Effect of Buffer on the Pyranine Dynamics. The only observed molecule is the pyranine anion, and the rate of its reprotonation is the basis for deducing the protonation of the various proton-binding sites present in the solution. As a first step, we shall demonstrate how proton acceptors, which are present in the reaction mixture, modulate the evolution of the observed signal. The experiments were carried out using small, free-diffusing buffer molecules formate (pK = 3.75), acetate (pK = 4.75), imidazole (pK = 6.95), and trimethylamine (pK = 9.81).

The effect of buffers on the pyranine reprotonation dynamics is presented in Figure 1, where the reprotonation kinetics of the pyranine were measured in the presence of increasing concentrations of acetate (panel A) and imidazole (panel B). As clearly seen in the figure, the shape of the curves varies with the concentration of the buffer and its pK value.

The acetate anion is an effective competitor for free protons, and the initial rate of the pyranine protonation decreases with increasing acetate concentrations. Once protonated, the acetate retains the proton in a bound state for 3−4 μs, which is its intrinsic dissociation time (*28*). As long as the proton is covalently bound, the pyranine can be reprotonated only by a collisional reaction with a protonated acetic acid molecule that is orders of magnitude slower than its reaction with free protons. Upon dissociation of the acetic acid, the competition for the proton between the acetate and the pyranine is resumed, and at high acetate concentrations, the relaxation of the pyranine is longer.

The more alkaline buffer imidazole affects the pyranine's dynamics in a different way.

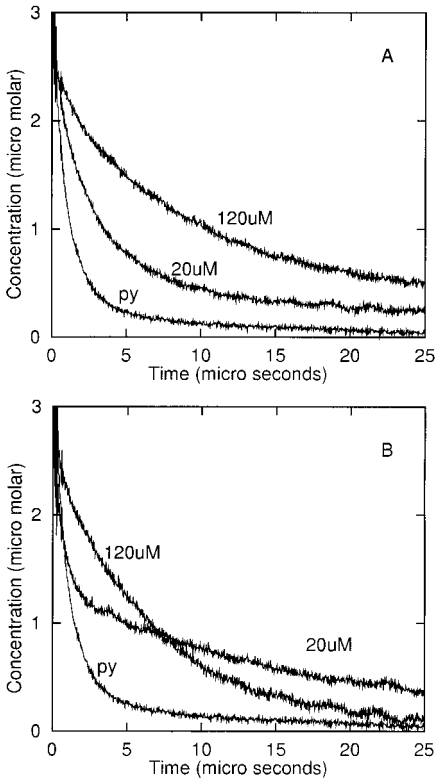

FIGURE 1: Effect of buffers on the reprotonation dynamics of pyranine. The reaction mixture contained an aqueous solution of pyranine (20 μM) and varying concentrations of buffers at pH 7.4, all in 100 mM NaCl. The reaction was initiated by a laser pulse (1.6 mJ, $\lambda = 355$ nm, 3 ns fwhm) that generated equal concentrations of free protons and pyranine anion. The reprotonation of the pyranine anion was followed over time at a λ of 458 nm. The traces are the average of 1000 consecutive pulses delivered at 10 Hz. Panels A and B depict the dynamics as measured with acetate and imidazole, respectively, and the concentrations of the buffers are indicated in the figure.

At the pH of the measurement (7.4), the imidazole exists as a mixture of two states: imidazolium (ImH^+), which can act as a proton donor for the pyranine, and imidazole, which is a proton acceptor. Accordingly, two parallel reactions will follow the perturbation: the imidazole will compete with the pyranine for the free protons, while the imidazolium will react in a collisional proton transfer reaction with the pyranine anion generated by the laser pulse. Thus, the dynamics in the presence of imidazole will vary with its concentration and its initial state of protonation. As seen in Figure 1B, at a low concentration the imidazole hardly affects the initial relaxation of the pyranine, but after some 5 μs, a slower relaxation is imposed. At higher imidazole concentrations, the capacity of ImH^+ to serve as a proton donor is augmented and the relaxation of the pyranine is fast.

Compounds that are more acidic than acetate (such as formate, p$K = 3.75$) or more basic than imidazole (such as trimethylamine, p$K = 9.81$) were found to have no effect on the measured dynamics (data not shown). The formate anion retains the bound proton for a time too short to modulate the kinetics of the reaction, while the basic compound is initially protonated and cannot compete for free protons. However, as such compounds are more basic than pyranine, they will not transfer their proton to the dye.

The study of binary mixtures, consisting of pyranine and buffers, clearly demonstrates that the shape of the chemical relaxation varies with the nature and concentration of the buffer. In a system containing protein, the relaxation of the perturbation is more complex as on every protein molecule there are many nonidentical proton-binding sites, each of which reacts independently with the discharged protons.

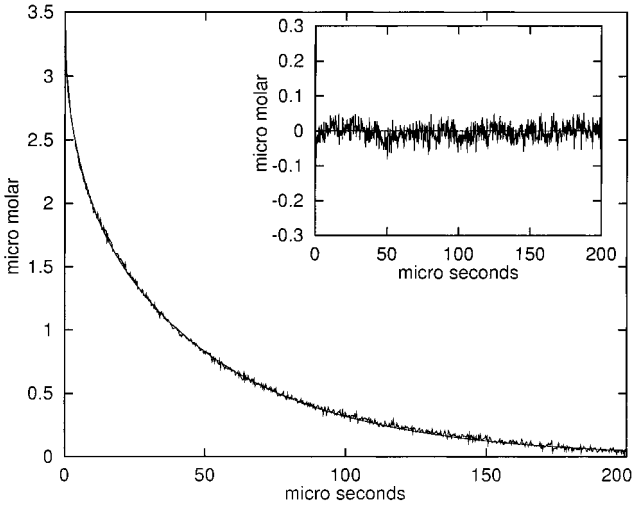

FIGURE 2: Reprotonation of pyranine in the presence of wild-type bacteriorhodopsin. The reaction was measured as described in the legend of Figure 1 (with the omission of 100 mM NaCl from the reaction mixture) in the presence of 17.4 μM pyranine and 20 μM wild-type bacteriorhodopsin at pH 7.3. The experimental curve was reconstructed by numeric integration of the differential rate equations that are pertinent to the system, using the parameters given in Table 2. The inset shows the deviation of the predicated function from the experimental signal.

Proton Binding Properties of Wild-Type Bacteriorhodopsin. The identification of the effect of a single carboxylate replacement in the BR molecule on the relaxation dynamics of the pyranine relies on the accuracy of the reconstruction of the standard signals measured with the wild-type protein. Accordingly, the next stage of this study was aimed at defining the accuracy of the kinetic and thermodynamic parameters characterizing the proton-binding sites of the native BR. The protonation of pyranine, in the presence of the wild-type protein, was recorded for many independent kinetic measurements, which were gathered when the concentrations of the protein and pyranine and the prepulse pH were varied independently. The results were subjected to kinetic analysis as described in Materials and Methods. This analysis was carried out as a re-evaluation of the accuracy of the parameters that were determined with the fluorescein-labeled BR preparations (*1*, *16*, *17*) and for determining the extent to which the parameters determined by the analysis of a single observed dye were consistent with those determined while monitoring both the pyranine and the bound fluorescein.

Figure 2 depicts an experimental curve and its reconstruction. The excellent quality of the fit is shown in the inset, where the deviation of the predicted function from the measured signal is presented. Except for a minor deviation ($\sim$3% of the amplitude) during the first $\sim$4 μs, the reconstruction fits the measured data within the limits set by the electronic noise. The fitting of a single kinetic record can be attained within a wide range of variance of the rate constants. The reconstruction of many experiments, gathered under varying initial conditions, by a single set of parameters is a more restraining, leading to a narrower variance of the

Table 2: Kinetic and Thermodynamic Parameters Characterizing the Dynamics of Proton Transfer between the Bulk and Surface of the Wild-Type Protein[a]

	N	p*K*	X + H^+	X + D38	X + D36	X + ϕO^-
ϕOH	1	7.7 ± 0.1	(7.3 ± 0.4) × 10^{10}	*≤3.0 × 10⁸*	*≤5.0 × 10⁹*	NA
D38	1	6.5 ± 0.1	(0.5 ± 0.1) × 10^{10}	*NA*	*≥1 × 10¹¹*	≤3 × 10^8
D36	1	4.5 ± 0.1	(1.5 ± 0.2) × 10^{10}	*≥1 × 10¹¹*	*NA*	≤5 × 10^9
cluster	3	5.5 ± 0.05	(4.0 ± 0.65) × 10^{10}	*(6.0 ± 1.1) × 10⁹*	*≤1 × 10¹⁰*	(4 ± 0.3) × 10^9
$COO_{ext.}$	1	5.1 ± 0.3	(0.5 ± 0.3) × 10^{10}			(9 ± 2) × 10^9

[a] The experiments were carried out at three pyranine concentrations (17.4, 23, and 28 μM) and varying pH values. The analysis fits 57 independent measurements. The rate constants are given in units of M^{-1} s^{-1}, except those of the virtual second-order reactions that are typed in italics.

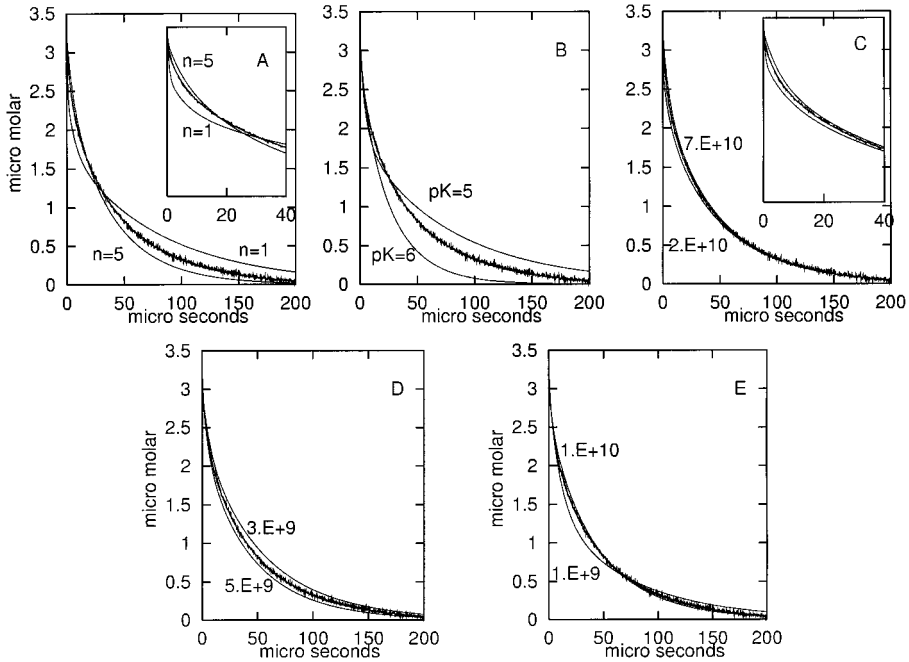

FIGURE 3: Effect of the various parameters on the shape of the reconstructed dynamics. Each frame depicts a single experimental curve with three reconstructed dynamics, where one of the parameters, characterizing the cluster, varies within the range indicated in the legend and marked in the figure. All other parameters were set as in Table 2. (A) The number of residues assigned to the cluster (n = 1, 3, and 5). The inset shows the expansion of the first 40 μs. (B) The pK of the cluster (pK = 5.0, 5.5, and 6.0). (C) The rate of protonation of the cluster ($k = 2 \times 10^{10}$, 5×10^{10}, and 7×10^{10} M^{-1} s^{-1}). The inset shows the expansion of the first 40 μs. (D) The rate of proton transfer between the cluster and the pyranine anion ($k = 3 \times 10^9$, 4×10^9, and 5×10^9 M^{-1} s^{-1}). (E) The rate of proton transfer between the cluster and D38. These rate constants are of virtual second-order reactions ($k = 1 \times 10^9$, 5.5×10^9, and 1×10^{10}).

rate constants. According to our accumulated experience (*29*), when more than 15 experimental curves are fitted by one set of parameters, the variance in the rate constants is sufficiently narrow to differentiate between two types of cytochrome *c* that differ by a single charged residue on their surface. In the study presented here, for each mutated protein, the analysis was carried out for 16 and up to 50 independent observations, achieving a high level of redundancy. The standard deviation of the rate constants, as calculated for the whole population of fitted curves, was ~20% of the mean value or even lower.

The quantitation of the kinetic and thermodynamic parameters characterizing the wild-type protein was based on 57 experimental curves that were all fitted by the rate constants listed in Table 2, with the same quality as in the inset of Figure 2. The values given in the table are a set of parameters that fit all measured signals within the margins set by the noise level. These values are also consistent with the parameters derived from the fluorescein-labeled bacteriorhodopsin preparations (*1*, *17*).

As the dynamics are controlled by the parameters given in Table 2, it was necessary to establish how each of them affects the dynamics and to what extent the modulation of the curve's shape by one parameter differs from the effect of the others. These calculations are presented in Figures 3−5. In each figure, there is an experimental curve and three reconstructions of the signal: the best-fit curve (obtained by the values given in Table 2) and two others where one of the parameters is varied above and below its best-fit value.

Three-Carboxylate Cluster. The most dominant proton acceptor on the BR surface has been shown to be a cluster of three carboxylates at the cytoplasmic face that, due to the merging of their coulomb cages, generates the strongest proton-attractive site on the BR surface (*1*, *16*, *17*). Figure 3 summarizes the effects of the kinetic and thermodynamic parameters of the cluster on the observed dynamics. Panel A depicts how varying the number of residues (from 1 to 5) affects the dynamics. The effect of the cluster's size on the dynamics changes during the observation time. In the short time range (see the inset of panel A), a small cluster will be a less effective competitor for free protons, with fast relaxation of the pyranine. On the other hand, a large cluster will better trap the discharged protons, leading to a slower reprotonation of the free dye. During the later phase of the

reaction ($t \geq 30$ μs), the mechanistic role of the cluster is inverted and it functions also as a proton donor to the dye. Accordingly, a large cluster will be a better donor, leading to faster relaxation during the late phase of the reaction.

The p*K* of each residue is defined as the ratio of the rate constants of its protonation and dissociation. Consequently, the kinetic analysis can determine the p*K* of a site, even when the pH of the measurements is far from its p*K* value. Thus, the evaluation of the cluster's contribution to the pyranine relaxation can be investigated by both the effect of the p*K* value (Figure 3B) and the rate constant of its reaction with free protons (Figure 3C). The best fit for the experimental curves, measured with the wild-type protein, was obtained within a very narrow range of p*K* values (5.5 ± 0.05). Either higher or lower values distort the fit beyond the noise level. Reconstructed dynamics that were carried out with a p*K* of >5.5 generated curves where the protein exhibited a reduced capacity to compete for and retain free protons. A cluster with a high p*K* will be in a protonated state before perturbation and will thus have a lower buffer capacity and a higher efficiency in acting as a proton donor with respect to the more basic pyranine anion (p$K = 7.7$ under the experimental conditions). A cluster with a lower p*K* has a different kinetic feature, and after a fast initial phase, the relaxation of the pyranine is slowed. Generally, the p*K* of the cluster modulates the reprotonation dynamics mostly at the time frame of $\sim$50 μs until the end of the observation. On the other hand, the rate of protonation of the cluster modulates the initial phase of the reaction, as shown in Figure 3C and its inset. Accordingly, the fitting of the experimental signal by the reconstructed curves can be used to determine the p*K* of the cluster and its rate of protonation.

The reprotonation of pyranine in the presence of bacteriorhodopsin is a sum of two pathways: a collisional proton transfer from the protein to the pyranine and a reaction with protons that spontaneously dissociated from the protein. The former pathway is the dominant one. Figure 3D demonstrates the sharpness of the dependence of the relaxation on the magnitude of the collisional pathway; varying the rate of the reaction within a narrow range ($3-5 \times 10^9$ M^{-1} s^{-1}) suffices to shift the reconstructed curves from above to below the experimental one. Careful analysis of the 57 measured curves narrowed the range of this rate constant to (4.0 ± 0.3) $\times$ 10^9 M^{-1} s^{-1}.

The last reaction through which the cluster modulates the reprotonation dynamics of pyranine is the proton transfer from the cluster to the carboxylate of D38 that, due to its high p*K* (see below), should have a longer dissociation time (*28*). Thus, a fast proton transfer from the cluster to D38 will affect the relaxation time of the pyranine. As shown in Figure 3E, this reaction modulates the curvature of the line by a mode that is not attained by the other parameters. The rate constant of the proton exchange reaction reflects the proximity of the two sites, and its magnitude is quantitated by a virtual second-order reaction (*19*). The mechanism of the reaction is a proton exchange through the solvent, but due to the proximity of the reactants, the probability of proton transfer from the donor to acceptor is larger than the dispersion of the proton into the bulk. Accordingly, the virtual second-order rate constants can be larger than the diffusion-controlled rate constants, but the units of M^{-1} s^{-1} are not applicable. The carboxylate moieties of residues D36 and D38 are only 5.4 Å apart (*11*) and carry out proton exchange between them with a virtual second-order reaction at a rate constant of 10^{12} (in this publication, all virtual second-order reactions are printed in italics) (*19*). For sites that are more remote, the virtual second-order rate constant is smaller. When the value is $<10^9$, it means that the proximity enhancement is no longer effective, and the mechanism is a simple dissociation followed by dispersion and diffusion through the bulk. As demonstrated in Figure 3E, the reaction between the cluster and D38 should be larger than 10^9.

Dynamics Features of D38. Besides the cluster, the other proton-binding sites on the cytoplasmic side of BR are D36 and D38. Both residues were identified as proton-binding sites on the protein through the quantitative analysis of the protonation dynamics of a fluorescein molecule attached to either the D36C or the D38C mutant (*1*, *16*, *17*). In the study presented here, where the pyranine reprotonation dynamics are the only measured signal, the contribution of D36 to the dynamics is rather small. Accordingly, we were satisfied to note that the kinetic and thermodynamic parameters previously assigned to D36 were consistent with the present reconstructions.

The carboxylate of D38 is the native proton donor to D96 during the M, N, and O steps of the photocycle (*18*). The p*K* of D38 was deduced, on the basis of kinetic analysis of protonation dynamics of a fluorescein residue attached to the D36C mutant, to be 6.5 (*1*), and because of that, it should affect the reprotonation of the pyranine. Figure 4A depicts the effect of the p*K* of D38 on the reconstructed dynamics of the wild-type protein. The three curves, which were calculated for p*K* values of 6.0, 6.5, and 7.0, exhibit almost identical dynamics during the first 20 μs, but with the progression of time, the reaction pathway reflects it dependence on the p*K* and the curves spread out. The pronounced dependence of the shape on this p*K* allowed us to determine the p*K* of D38 with a high level of accuracy. The high p*K* of this residue (6.5) is in accord with its location inside the proton-conducting channel of the BR, where the low dielectric constant of the environment favors the protonated, uncharged state of the carboxylate. The limited exposure of D38 to the bulk is also deduced by the rate constant of proton transfer between the carboxylate and the free-diffusing pyranine anion. The proton exchange reaction with the cluster will eventually lead the proton to D38 that, thermodynamically, is the most attractive site on the cytoplasmic side on the protein. As a result, toward the late phase of the relaxation, the reprotonation of the pyranine is at the expense of deprotonation of D38. As seen in Figure 4B, the relaxation dynamics of the pyranine necessitate that the accessibility of the dye, with a gyration radius of $\sim$5 Å, should be rather small and that the rate constant (k) should have an upper limit of $\leq 10^6$ M^{-1} s^{-1}.

Carboxylates of the Extracellular Face of Bacteriorhodopsin. Measurements carried out with wild-type BR labeled at K129 (*17*) revealed that, of the five carboxylates on the extracellular side of BR (E1, E9, E74, E194, and E204), only one proton-binding site was seen to affect the protonation dynamics of the fluorescein. In the analysis presented here, we adhered to the previous conclusions and verified that incorporation of the kinetic parameters assigned to the extracellular carboxylate indeed complies with the present

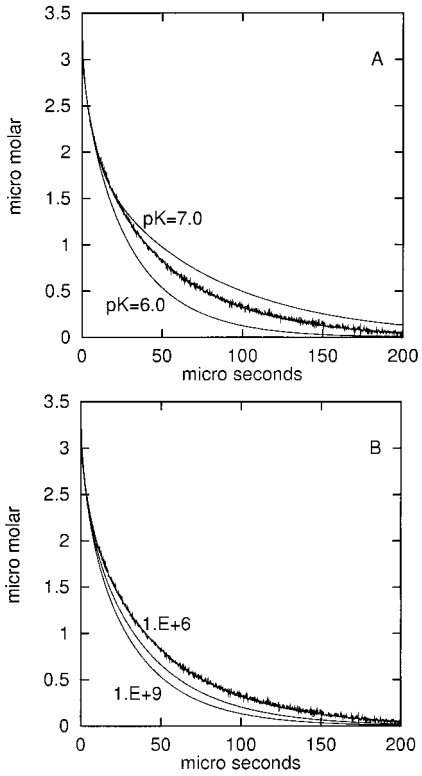

FIGURE 4: Effect of the various parameters on the shape of the reconstructed dynamics. Each frame depicts a single experimental curve with three reconstructed dynamics where one of the parameters, characterizing the carboxylate of D38, varies within the range indicated in the legend and marked in the figure. All other parameters were set as in Table 2. (A) The p*K* values of the residue were set to 6.0, 6.5, and 7.0 as marked in the figure. (B) The rate of proton transfer between D38 and the pyranine anion (*k*) was set to 1×10^6, 5.5×10^8, and 1×10^9 as marked in the figure.

measurements and reconstructions. The modulation of the pyranine signal by the extracellular carboxylate is rather feeble, yet as shown in Figure 5, the best fit of the measured curve is attained with one carboxylate per BR molecule. Reconstruction of the dynamics, assuming that the extracellular face carries either one or two carboxylates, causes systematic errors that extend beyond the noise level (see the inset). Using the same criteria, we estimated the p*K* of the reactive extracellular carboxylate to be 5.1 ± 0.3 (not shown).

Dynamics Measured in the Presence of Mutated BR. The data presented above demonstrate that the pyranine relaxation dynamics are very sensitive to the proton binding capacity of the protein, and for simultaneous fitting of a large number of measured signals ($n = 57$), the kinetic and thermodynamic parameters of the surface groups fall within narrow limits. These parameters, listed in Table 2, are defined as the wild-type parameters, and serve as the basis for the analysis of the kinetics measured with the mutants described in detail below. The signals, measured with the mutated protein, were first tested to see whether they could be simulated by the wild-type parameters, and when a good fit was not attained, the features of the surface groups were varied.

During the replacement of the surface carboxylates and after measuring the effect on the pyranine reprotonation dynamics, we observed three patterns of relaxation: (1) mutations where the relaxation of the pyranine signal was identical with that of the wild type (D102C and E74C), (2) mutations that specifically affect only the three-carboxylate cluster on the cytoplasmic surface, and (3) mutations that caused major modulation of the proton binding capacity of the protein's surfaces. The third group of mutants will not be discussed herein.

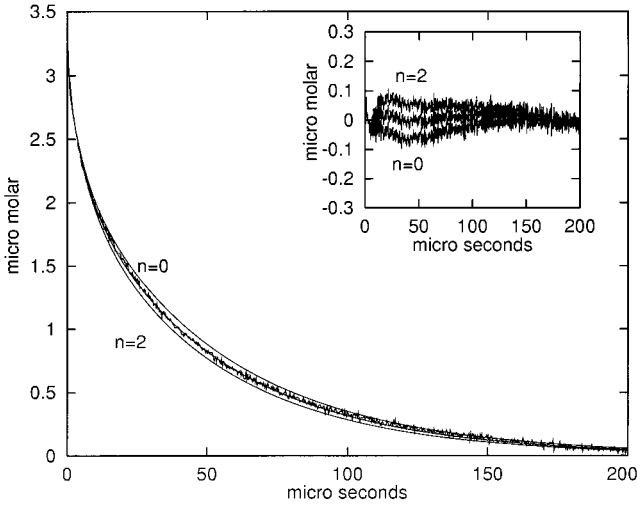

FIGURE 5: Effect of the number of extracellular carboxylates on the reconstructed dynamics. Three reconstructed curves are presented in this figure, calculated for one, two, or three carboxylates on the extracellular face. All other parameters were set as in Table 2. The inset shows the deviation from the experimental signal.

The analysis of the signal measured with the mutated proteins was based on the parameters needed for the reconstruction of the wild-type protein using the following algorithm. At first, the reconstructions were carried out using the standard parameters of the wild-type protein (as in Table 2). If the parameters of the wild type generated a curve with slower relaxation dynamics, it was interpreted that the mutated protein had a smaller capacity to compete for the free protons and the kinetic features of the cluster were modified until a fair fit was obtained. Once that was achieved, a detailed analysis was carried out with refinement of all rate constants. Double mutants (like D104N/D38C) were analyzed by taking the parameters determined for the D104-less protein as a first approximation, and eliminating the kinetic parameters of D38 (as given in Table 2) from the kinetic scheme. In all cases, this modular operation was sufficient to obtain a fair reconstruction of the signal, and the parameters were later refined to obtain curves where the deviations were within the electronic noise level.

The results of the analysis of the transients measured with the mutated protein are listed in Table 3 that summarizes the rate constants and p*K* values of the carboxylate cluster on the cytoplasmic surface of the membrane. The analysis of the results also yielded rate constants and p*K* values for D36, D38, and the extracellular carboxylate. However, as their values were within the range of the wild-type parameters, they are not given in the tables. In the following section, we shall discuss how each mutation affected the reactivity of the cytoplasmic side of the membrane.

Role of D102 and D104 in the Dynamics of Bulk−Surface Proton Transfer. The two carboxylates, D104 and D102, are located on the cytoplasmic loop connecting helixes C and D, with a distance of 6.7 Å between their carboxylate moieties (*11*). When this proximity was considered, it was expected that their kinetic role would be the same. Yet, the two mutants (D102C and D104C) markedly differ in the

Table 3: Parameters of the Proton Transfer Reaction of the Cluster on the Cytoplasmic Surface of Various Mutants[a]

	sample	n[b]	cluster size	pK	$X + H^+$ (M^{-1} s^{-1})	$X + \phi O^-$ (M^{-1} s^{-1})
1	wild type	57	3	5.5 ± 0.05	$(4.0 \pm 0.6)(5) \times 10^{10}$	$(4.0 \pm 0.3) \times 10^9$
2	D102C	22	3	5.5 ± 0.05	$(5.0 \pm 0.9) \times 10^{10}$	$(3.0 \pm 0.8) \times 10^9$
3	D102N/D38C	34	3	5.5 ± 0.05	$(2.4 \pm 0.7) \times 10^{10}$	$(3.1 \pm 0.9) \times 10^9$
4	D104C	26	2	6.5 ± 0.05	$(3.9 \pm 0.3) \times 10^{10}$	$(5.0 \pm 0.5) \times 10^9$
5	D104N/D38C	26	2	6.0 ± 0.05	$(3.8 \pm 0.8) \times 10^{10}$	$(3.6 \pm 1.1) \times 10^9$
6	E161C	18	2	5.5 ± 0.05	$(4.3 \pm 0.5) \times 10^{10}$	$(3.2 \pm 1) \times 10^9$
7	E161N/D38C	18	2	5.5 ± 0.05	$(3.1 \pm 0.8) \times 10^{10}$	$(2.2 \pm 1) \times 10^9$
9	EDC-treated	16	1 + 1	5.5 ± 0.05	$(1.7 \pm 0.3) \times 10^{10}$	$(1.8 \pm 0.8) \times 10^9$
8	E234Q/D38C	26	1 + 1	5.5 ± 0.05	$(2.1 \pm 1.1) \times 10^{10}$	$(1.0 \pm 0.5) \times 10^9$
10	D36C	35	3	5.6 ± 0.05	$(7.7 \pm 0.6) \times 10^{10}$	$(2.6 \pm 0.9) \times 10^9$
11	D36C/D38R	25	3	5.3 ± 0.05	$(0.9 \pm 0.12) \times 10^{10}$	$(1.0 \pm 0.5) \times 10^8$

[a] The values are those characterizing the cluster. All other rate constants are within the limits set in Table 2. [b] n denoted the number of experiments carried out with each preparation that was reconstructed.

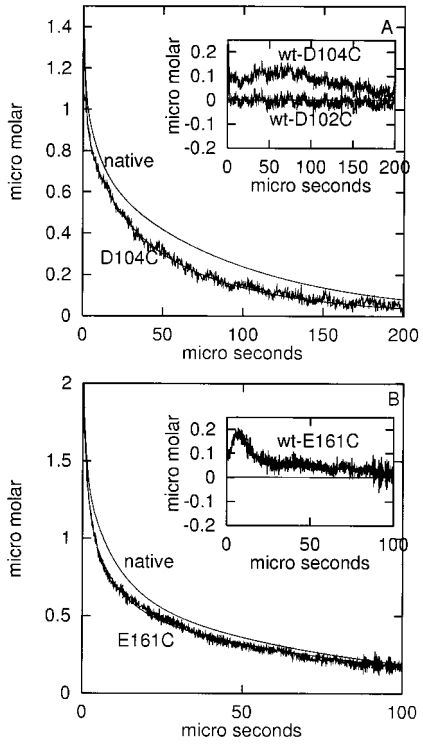

FIGURE 6: Reprotonation dynamics of pyranine in the presence of the D104C, D102C, and E161C mutants of bacteriorhodopsin. (A) The reaction with the D104C mutated protein (2.7 μM) was measured as described in the legend of Figure 2 at pH 7.06 and in the presence of 17.4 μM pyranine. The fitting of the D104 signal was carried out with the parameters given in Table 3. The wild-type signal is represented by its reconstructed dynamics. The inset depicts the deviation of the signals measured with the D102C and D104C mutants from the curve generated by the wild-type parameters. Note that the dynamics measured with the D102C mutant exhibit no systematic deviations from the values calculated with the wild-type parameters. (B) The E161C mutant (4.3 μM) was suspended at pH 7.3 in the presence of 17.3 μM pyranine, and the absorbencies were measured at 458 nm. The parameters that simulate the signal are given in Table 3. For comparison, the wild-type signal is represented by its simulated dynamics. The deviation of the measured signal from the wild-type reconstructed dynamics is given in the inset.

reprotonation dynamics of the pyranine.

The transients measured with D102C were readily reconstructed by the parameters determined for the wild-type protein, as shown in the inset of Figure 6A, which depicts the difference between the experimental signal and dynamics reconstructed by the wild-type parameters. Apparently, the elimination of the carboxylate residue at position 102 has no effect on the rate of proton uptake from the bulk, as detected by the pyranine anion. A full analysis of the D102C mutant was carried out. The dynamics of 22 independent measurements, each under different initial conditions, were reconstructed by a set of parameters that did not deviate significantly from those of the wild type (compare rows 1 and 2 of Table 3). The carboxylate moiety of D102 is well exposed to the bulk, and is likely to react with free protons. Thus, its negligible contribution to the reaction we measured suggests that its pK is downshifted by the positive charge of K159 to a level sufficiently low so as not to modulate the microsecond dynamics of bulk−surface proton transfer, which is reminiscent of the vanishing effect of formate anion on the reprotonation dynamics of pyranine.

Another mutant, D102N/D38C, was employed for evaluating the role of D102 in the bulk−surface proton transfer reaction. In this protein, an amide residue blocks the D102 carboxylate, and the negative charge of D38, located at the entry to the proton-conducting channel (*18*), was also removed. Taking the wild-type parameters (which are very close to that of D102C) and omitting the reaction in which D38 participates from the kinetic scheme yielded the reconstruction of the transients. This modular operation was sufficient to generate curves which were close enough to the measured signals so that only a minor adjustment of the rate constants was required to reconstruct 34 independently measured signals (see row 3 in Table 3). The elimination of the negative charge of D38 somewhat reduced the surface charge density near the reaction cluster, and a lower rate constant of protonation was needed for the reconstruction of the signals. Thus, the results gathered with D102C and D102N/D38C indicate that the carboxylate at position 102 is not a member of the three-carboxylate cluster of the native protein.

The carboxylate moiety of D104 located in the BR state of the protein, only a few angstroms apart from D102, has a major function in the bulk−surface proton transfer reaction of the BR protein. The reprotonation dynamic of the pyranine, as measured in the presence of the D104C protein (Figure 6A), is much faster than that measured with the native BR (represented by the reconstructed curve). A faster relaxation implies that the elimination of the D104 carboxylate reduced the capacity of the protein to compete with the pyranine for the free protons, and as a result, the pyranine regains its initial state of protonation within a shorter time period. The systematic deviation of the signal, measured for D104C, from the reconstructed curve calculated by the

parameters of the wild type (see the inset of Figure 6A), necessitated fitting of the signals measured with the mutant with their own specific rate constants. These parameters are given in row 4 of Table 3. Reducing the number of carboxylates in the cluster from three to two and assigning them a higher p*K* with value yielded the fitting of 26 transients, each measured under different initial conditions. Thus, it appears that D104 is a member of the three-carboxylate cluster on the cytoplasmic side of the membrane. The fact that one component of the cluster was removed while the remaining two carboxylates maintain a fast rate of protonation (3.9×10^{10} M^{-1} s^{-1}) implies that the remaining two carboxylates are still close to one another so that the pair has a higher attractivity for free protons than that of two, noninteracting carboxylates. Still, the higher p*K* value and a somewhat faster proton transfer between the two carboxylates and the pyranine anion suggest that the surrounding environment was slightly modified by the removal of D104.

Experiments were also carried out with the D104N/D38C double mutant. The reconstruction of 26 independent kinetic tracings led to a solution, which was based on the parameters of the D104C system, with the omission of the reaction in which D38 is involved. The values were subjected to final refinement until the deviation of the reconstructed curve from the experimental one was within the electronic noise level.

Role of E161 in the Cluster Function. The kinetics measured with the mutant E161C significantly deviated from those of the wild type, resembling the curves recorded with D104C (Figure 6B). Analysis of 18 independent experimental observations led to the solution given in row 6 of Table 3. The analysis indicates that the removal of the negative charge at the site of residue 161 affects the proton binding capacity of the mutant in a mode similar to the removal of D104. In both mutants, the cluster is reduced to two carboxylates, but still retains the high rate of protonation and a p*K* value of >5. Experiments with a double mutant (E161Q/D38N) were carried out and analyzed. The solution was consistent with the set of parameters determined for E161C with the omission of the kinetic and thermodynamic parameters associated with D38 (row 7 of Table 3).

Residue E161 is located on the loop connecting helix E with helix F. This loop had not been resolved in some models (*30*), while in others (*11*), it is quite blurred, with a high temperature factor. Recent EPR studies (*31*) indicated that the loop forms a short α-helix structure running parallel to the membrane surface. Spin labeling of the E161C mutant (*32*, *33*) indicated that the residue is exposed to the bulk, which is in accord with the results of the study presented here.

On the basis of our kinetic analysis, and supported by the EPR measurements, we conclude that E161 is a member of the three-carboxylate cluster of the wild-type protein.

Involvement of the Carboxylate on the C-Terminal Tail in the Cluster Function. The third residue associated with the cluster is E234, which is located only two residues from the last structurally resolved amino acid (*11*). The first identification of E234 as a component of the cluster was based on EDC labeling experiments. Treatment of BR with EDC exclusively modifies the carboxylates of E74, D38, and E234 (*26*). The first one has no effect on the pyranine relaxation dynamics (S. Checover, unpublished results).

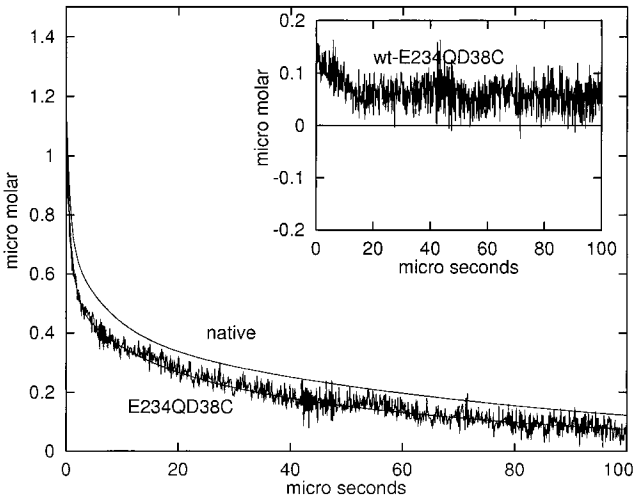

FIGURE 7: Dynamics of reprotonation of pyranine in the presence of the E234Q/D38C double mutant. The PM (4.0 μM protein) was suspended in water at pH 7.7 in the presence of 18.8 μM pyranine and measured as described in the legend of Figure 2. The measured signal was reconstructed by the parameters given in Table 3. For comparison, the wild-type signal is represented by its simulated dynamics. It should be noted that the relaxation of the mutant is faster than that of the wild type, indicating a reduction in the buffer capacity of the protein.

Residue D38 has a distinct effect on the measured dynamics and is not a component of the cluster (its kinetic features are documented above).

The signals measured with the EDC-treated protein (not shown) are characterized by a fast relaxation of the pyranine signals, indicating a reduction of the proton binding capacity. The diminished capacity of the cluster to react with free protons is in accord with the observation of Dencher and Verclas (unpublished results), who found that the EDC-treated BR regains protons from the bulk at a significantly slower rate than does the wild-type protein.

The reconstruction of the measured signals could not be attained by the wild-type parameters with the omission of the contribution of D38 from the reaction mechanism, as was sufficient in the case of the D102N/D38C and D104N/D38C double mutants. Thus, E234 appears to be an active component of the proton-attracting cluster. The analysis of 26 independent measurements was attained by parameters listed in row 8 of Table 3. Further verification of E234 as a member of the cluster was attained by measurements with the E234Q/D38C double mutant (Figure 7). The observed dynamics were practically indistinguishable from those of the EDC-treated enzyme, and were perfectly fitted by the same parameters determined for the EDC-treated protein.

The kinetic features of the two preparations are consistent with two carboxylates that react with a rate constant *k* of $1.7-2.0 \times 10^{10}$ M^{-1} s^{-1}. This value is only 50% of a rate measured for the intact cluster or for the D104C and E161C mutants. The rate constants of the protonation of the surface carboxylates of the EDC and E234Q/D38C mutants are compatible with the protonation rate of a single carboxylate on a structure of a membrane or a micelle (*34*). It seems that the elimination of the negative charge of E234 fragments the overlap in the coulomb cage and the three-carboxylate cluster was severely damaged, causing it to consist of two independent carboxylates. That feature was not noticed in the case of the other two residues (D104 and E161). When

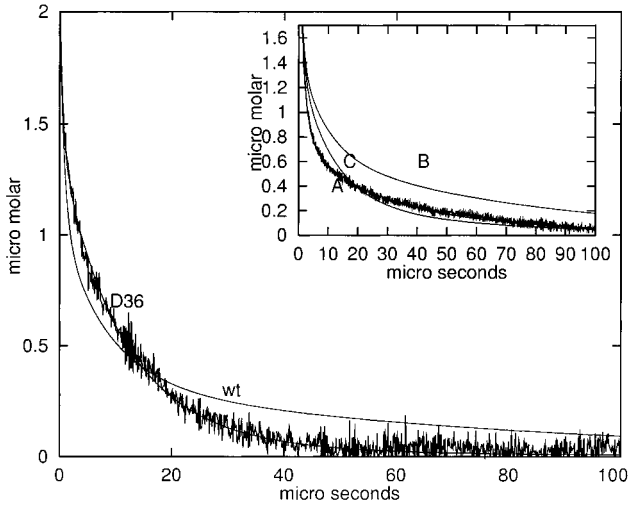

FIGURE 8: Dynamics of the reprotonation of pyranine in the presence of the D36C and D36C/D38R mutants. The PM (3.8 μM protein) was suspended in water at pH 7.3 in the presence of 22.7 μM pyranine. The main frame shows the signal measured with the D36C mutant with its reconstructed dynamics using the parameters listed in Table 3. The inset shows the dynamics measured with the D36C/D38R double mutant. Curve A corresponds to the measured signal and its reconstructed dynamics using the parameters given in Table 3; curve B represents the reconstructed dynamics of the wild-type protein, and curve C is the reconstructed dynamics of the wild-type protein when both D36 and D38 were omitted form the kinetic model.

the fact that the distance between them is ~16 Å is considered, the E234 may be located as a bridge between them, thus linking the three into one effective cluster.

Modulation of the Cluster by Nearby Charges. The special kinetic features of the three-carboxylate cluster of the native protein are attributed to the proximity between the residues that overlap their coulomb cages. However, examination of the kinetic parameters of the cluster indicates that its features are modulated by the charges of D36 and D38 located at the orifice of the proton channel (*1*, *18*).

As shown in Figure 8, the elimination of the negative charge of D36 caused a peculiar modulation of the pyranine relaxation dynamics, in a mode compatible with enhanced reaction of the protein with the free protons. To reconstruct the measured signal, the rate constant of the cluster protonation had to be almost doubled (row 10 of Table 3).

The interaction between the charges, at the orifice of the proton-conducting channel, with the three-carboxylate cluster can be detected by the rate constants of the cluster as determined for the two double mutants, D102N/D38C and E161Q/D38C (Table 3). In both cases, the reaction of the cluster with free protons is slower than that of the wild type. Accordingly, it was expected that replacement of the negative charge of D38 with a positive one (as in the D36C/D38R) will further reduce the proton attractivity of the domain.

The dynamics measured with the D36C/D38R mutant are presented in the inset of Figure 8, and the rate constants of the cluster's reactions with free protons and the pyranine anion are given in row 11 of Table 3. The mutant appears to have a much lower capacity to compete for free protons, and the relaxation of the pyranine is much faster than that assessed in the presence of equal concentrations of the wild-type protein (curve B) or as expected by the elimination of the contribution of both D36 and D38 from the wild-type parameters (curve C). Thus, the lower proton binding capacity is due to the positive charge of arginine replacing the anion of D38. The kinetic analysis of 25 measurements indicated (Table 3) that the positive charge of the arginine had disentangled the cluster with a subsequent loss of all its kinetic advantage. In the D36C/D38R mutant, the carboxylates of the cluster function as three independent moieties, each reacting with free protons with a rate constant of 0.9 $\times$ 10^{10} M^{-1} s^{-1}, which is a typical value for a single surface carboxylate (*27*, *35*). The positive charge, inserted a little below the protein−water interface, disrupted the charge cooperation between the three residues.

DISCUSSION

The previous proton pulse experiments, carried out with bacteriorhodopsin, indicated that the cytoplasmic side of this membrane protein is characterized by a high-affinity proton-binding site consisting of three carboxylates (*1*, *17*). Such unique kinetic features can serve as a structural marker, indicating the proximity between the carboxylates. Considering that the interconnecting loops on the cytoplasmic surface of the enzyme are structurally poorly resolved, the kinetic observation can assist in identifying some of the transient conformations of the protein. For this reason, we investigated a large number of mutants, in a search for those residues whose elimination will reduce the capacity of the cluster to react with free protons.

The experimental procedure was to challenge each mutant by a brief proton pulse from the aqueous bulk phase and from the reprotonation dynamics of the pyranine, to deduce the capacity of the protein to react with free protons and to retain them on its surface. By this mode of observation, we could avoid modulation of the protein's surface caused by attachment of H^+-reporter groups.

The reconstruction of the dynamics measured with the wild-type protein yielded a set of rate constants and p*K* values with sufficient accuracy to state with certainty that some of the mutants exhibit kinetic properties that differ from those of the wild type. What is more, the observation that two mutations [D102C (this study) and D74C (S. Checover, unpublished results)] were described by the wild-type parameters is evidence that each not mutation alters the kinetic properties of the enzyme. This negative observation implies that when the parameters deviated from those of the wild-type protein, there is a structural chemical reason for it.

Of the three residues forming the cluster, only D104 is structurally well resolved. The second carboxylate of the cluster, E161, is located on the less resolved EF loop (*30*). The third component of the cluster, E234, is located on the C-terminal section of the protein, which until now, had been resolved only for the M state of the protein (PDB entry 1CWQ). A comparison of the interaction between the charged residues on the cytoplasmic surface reveals gross deviations between the two states of the enzyme. Thus, the interrelation between E234 and the other carboxylates of the cluster must be derived from the kinetic analysis. The kinetic features of the cluster are consistent with a transient structure where the coulomb cages of the carboxylates merge to a single high-proton attractive site. What is more, the elimination of D104 or E161 reduces the cluster to a two-carboxylate

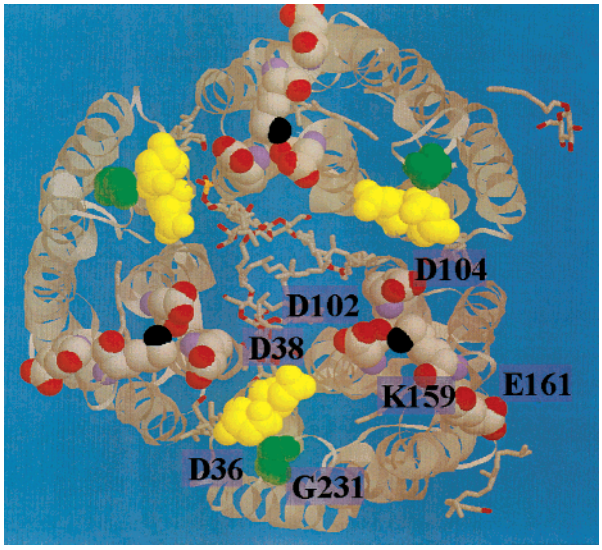

FIGURE 9: Cytoplasmic surface of the bacteriorhodopsin trimer based on the model of Essen (*11*), highlighting the residues investigated in the study presented here. The two residues at the entrance to the proton-conducting channel (D36 and D38) are colored yellow, and the distance between the carboxylates is 5.4 Å. D102, D104, and E161 are given in the CPK colors. Please note that the basic nitrogen of K159 (black) is closer to the carboxylate of D102 (3.9 Å) than to that of D104 (5.3 Å) The distance from the carboxylate moieties of D104 to that of E161 is 16.1 Å; the distance from the carboxylate of D104 to D38, on the same monomer, is 15 Å, and the distance from D104 to D36 of the next monomer is only 9.2 Å. Gly231, which is the last resolved residue next to the C-terminus, is in green. Somewhere, within a radius of ~10 Å, residue E234 may be located. According to that assignment, the carboxylate of E234 is located between the carboxylates of D104 and E161, while the proton picked by the cluster is transferred either to the proton entry domain of the same monomer or, via D104, to the D36, D38 domain of the next, clockwise protein.

structure, while removal of E234 abolished the proton attractor function of the site. Accordingly, the E234 should be placed between the two other carboxylates. On the basis of these data, we can speculate about the possible location of E234 with respect to the structure of the trimeric arrangement of the bacteriorhodopsin. Figure 9 depicts the BR trimer as seen from the cytoplasmic side of the membrane. The proton entry domain of the channel is marked by D36 and D38, colored in yellow, while the last residue next to the C-terminus is G231, colored in green. The other residues are colored according to the CPK code. Please note that the positive charge of K159 is very close to the carboxylate of D102, which accounts for its low p*K* value and it marginal effect on the transient protonation of the protein. D104 and E161 are too far apart to merge their coulomb cages. Yet placement of E234 between the two will form a set of three carboxylates that are close enough to function as a high-proton attractive cluster. The second clue for the position of E234 is that the cluster can function as an effective proton donor to a fluorescein residue attached to D36 (*1*), and that the kinetic properties of the cluster are coupled with the charges at the vicinity of the orifice of the proton channel. Thus, the elimination of the negative charge in D36C doubles the attractivity of the cluster, while insertion of a positive charge in D36C/D38R disrupts the cluster. Similarly, the neutralization of the charge on residue 38 (as in the D38C mutants) reduces the rate constant of the reaction of the cluster with free protons. This linkage suggests that the cluster is located close to the D36/D38 region on the cytoplasmic surface. Close examination of the structure depicted in Figure 9 implies that to satisfy this requirement, the cluster on monomer B should interact with the D36/D38 region of monomer A, which is much closer than within the same monomer (~10 vs ~15 Å, respectively). The fact that until now, and under all experimental conditions, the last section of the C-terminal region of the BR state of bacteriorhodopsin was not properly resolved may suggest that it can occupy more than one conformation, and that these forms rapidly alternate between states that are almost equipotential. Thus, the location deduced from the kinetic analysis implies that one of the possible configurations of the C-terminal section places E234 between D104 and E161 of one protein and the D36/D38 region of the counterclockwise neighbor at a sufficient frequency or probability to serve as an efficient proton-conducting link between the two proteins. The implication of the proton exchange reaction between monomers implies that the headgroups of the charged lipids may have a crucial role in the reaction, in accord with some recent observations (S. Checover and N. A. Dencher, unpublished results).

The results presented in this study probe the interconnections between the proton-binding sites on the surface of the BR state of the enzyme. We have demonstrated that the specific, probably transient, configuration of proton-binding sites endows the protein with an enhanced capacity to pick up protons from the bulk. It is likely that such a function, which is not essentially based on the same residues, may characterize the other states of the enzyme. On measuring the effect of carboxylate replacement on the photocycle, Brown et al. (*20*) had observed certain modulations of the M decay dynamics by some specific residues; D102N had no effect on the M decay rate, while D104N slowed the reaction by 50%. Similarly, while we noticed that the D36N mutation amplified the kinetic properties of the cluster, Brown et al. (*20*) reported accelerated protonation of the M state. Apparently, even though the time frames of our fast proton probing reaction and the photocycle measurements of Brown differ 100-fold, some similarities between the velocities are persistent.

Bacteriorhodopsin is a small, well-studied protein whose structure−function correlations are rapidly revealed. Yet the structural information is mostly derived from time invariant measurements, thus missing the role of the protein dynamics in the photocycle reactions. The fast proton transfer measurements are not the key for reconstruction of the physiological function of the protein; some of the photocycle steps are orders of magnitude longer than a simple proton transfer reaction. These studies are a measure of the transient configurations of the protein, and can reveal aspects undetected with the static presentations of the enzyme. The application of the time-resolved proton transfer kinetics for charting the relative distance between the proton-binding sites on the M state of the protein is currently under study.

REFERENCES

1. Checover, S., Nachliel, E., Dencher, N. A., and Gutman, M. (1997) *Biochemistry 36*, 13919−13928.
2. Grigorieff, N., Ceska, T. A., Downing, K. H., Baldwin, J. M., and Henderson, R. (1996) *J. Mol. Biol. 259*, 393−421.

3. Henderson, R., Baldwin, J. M., Ceska, T. A., Zemlin, F., Beckmann, E., and Downing, K. H. (1990) *J. Mol. Biol. 213*, 899−929.
4. Kimura, Y., Vassylyev, D. G., Miyazawa, A., Kidera, A., Matsushima, M., Mitsuoka, K., Murata, K., Hirai, T., and Fujiyoshi, Y. (1997) *Nature 389*, 206−211.
5. Mitsuoka, K., Hirai, T., Murata, K., Miyazawa, A., Kidera, A., Kimura, Y., and Fujiyoshi, Y. (1999) *J. Mol. Biol. 286*, 861−882.
6. Takeda, K., Sato, H., Hino, T., Kono, M., Fukuda, K., Sakurai, I., Okada, T., and Kouyama, T. (1998) *J. Mol. Biol. 283*, 463−474.
7. Luecke, H., Schobert, B., Richter, H. T., Cartailler, J. P., and Lanyi, J. K. (1999) *J. Mol. Biol. 291*, 899−911.
8. Sato, H., Takeda, K., Tani, K., Hino, T., Okada, T., Nakasako, M., Kamiya, N., and Kouyama, T. (1999) *Acta Crystallogr. 55*, 1251−1256.
9. Pebay-Peyroula, E., Rummel, G., Rosenbusch, J. P., and Landau, E. M. (1997) *Science 277*, 1676−1681.
10. Landau, E. M., and Rosenbusch, J. P. (1996) *Proc. Natl. Acad. Sci. U.S.A. 93*, 14532−14535.
11. Essen, L. O., Siegert, R., Lehmann, W. D., and Oesterhelt, D. (1998) *Proc. Natl. Acad. Sci. U.S.A. 95*, 11673−11678.
12. Belrhali, H., Nollert, P., Royant, A., Menzel, C., Rosenbusch, J. P., Landau, E. M., and Pebay-Peyroula, E. (1999) *Struct. Folding Des. 7*, 909−917.
13. Muller, D. J., Buldt, G., and Engel, A. (1995) *J. Mol. Biol. 249*, 239−243.
14. Muller, D. J., Sass, H. J., Muller, S. A., Buldt, G., and Engel, A. (1999) *J. Mol. Biol. 285*, 1903−1909.
15. Heymann, J. B., Muller, D. J., Landau, E. M., Rosenbusch, J. P., Pebay-Peyroula Buldt, G., and Engel, A. (1999) *J. Struct. Biol. 128*, 243−249.
16. Nachliel, E., and Gutman, M. (1996) *FEBS Lett. 393*, 221−225.
17. Nachliel, E., Gutman, M., Kiryati, S., and Dencher, N. A. (1996) *Proc. Natl. Acad. Sci. U.S.A. 93*, 10747−10752.
18. Riesle, J., Oesterhelt, D., Dencher, N. A., and Heberle, J. (1996) *Biochemistry 35*, 6635−6643.
19. Sacks, V., Marantz, Y., Aagaard, A., Checover, S., Nachliel, E., and Gutman, M. (1998) *Biochim. Biophys. Acta 1365*, 232−240.
20. Brown, L. S., Needleman, R., and Lanyi, J. K. (1999) *Biochemistry 38*, 6855−6861.
21. Gutman, M., and Nachliel, E. (1995) *Biochim. Biophys. Acta 1231*, 123−138.
22. Gutman, M., and Nachliel, E. (1997) *Annu. Rev. Phys. Chem. 48*, 329−356.
23. Tanford, C. (1957) *J. Am. Chem. Soc. 79*, 5348−5352.
24. Ferrando, E., Schweiger, U., and Oesterhelt, D. (1993) *Gene 125*, 41−47.
25. Oesterhelt, D., and Stoeckenius, W. (1974) *Methods Enzymol. 31*, 667−686.
26. Renthal, R. (1977) *Biochem. Biophys. Res. Commun. 77*, 155−161.
27. Yam, R., Nachliel, E., and Gutman, M. (1988) *J. Am. Chem. Soc. 110*, 2636−2640.
28. Gutman, M., and Nachliel, E. (1990) *Biochim. Biophys. Acta 1015*, 391−414.
29. Marantz, Y., and Nachliel, E. (1999) *Isr. J. Chem. 39*, 439−445.
30. Lanyi, J. K. (1999) *Int. Rev. Cytol. 187*, 161−202.
31. Steinhoff, H., Savitsky, A., Wegener, C., Pfeiffer, M., Plato, M., and Mobius, K. (2000) *Biochim. Biophys. Acta 1457*, 253−262.
32. Pfeiffer, M., Rink, T., Gerwert, K., Oesterhelt, D., and Steinhoff, H. J. (1999) *J. Mol. Biol. 287*, 163−171.
33. Rink, T., Pfeiffer, M., Oesterhelt, D., Gerwert, K., and Steinhoff, H. J. (2000) *Biophys. J. 78*, 1519−1530.
34. Nachliel, E., and Gutman, M. (1988) *J. Am. Chem. Soc. 110*, 2635.
35. Yam, R. (1988) in *The ion pumps: stucture, function and regulation* (Stein, W. D., Ed.) pp 279−282, Alan R. Liss, New York.

BI002574M